

Adverse Weather Conditions Augmentation of LiDAR Scenes with Latent Diffusion Models

1st Andrea Matteazzi^{1,2}
matteazzi@uni-wuppertal.de

2nd Pascal Colling²
pascal.colling@aptiv.com

3rd Michael Arnold²
michael.arnold@aptiv.com

4th Dietmar Tutsch¹
tutsch@uni-wuppertal.de

¹University of Wuppertal

²Aptiv Services Deutschland GmbH

Abstract—LiDAR scenes constitute a fundamental source for several autonomous driving applications. Despite the existence of several datasets, scenes from adverse weather conditions are rarely available. This limits the robustness of downstream machine learning models, and restrains the reliability of autonomous driving systems in particular locations and seasons. Collecting feature-diverse scenes under adverse weather conditions is challenging due to seasonal limitations. Generative models are therefore essentials, especially for generating adverse weather conditions for specific driving scenarios. In our work, we propose a latent diffusion process constituted by autoencoder and latent diffusion models. Moreover, we leverage the clear condition LiDAR scenes with a postprocessing step to improve the realism of the generated adverse weather condition scenes.

Index Terms—Data augmentation, Adverse weather, Latent diffusion models

I. INTRODUCTION

LiDAR-based applications such as 3D object detection must be reliable across different scenes and weather conditions. To achieve this degree of robustness, machine learning models need to be trained on a massive amount of feature-diverse data. For example, 3D object detection models may fail on detecting heavily occluded objects or false detecting clusters of snow as objects [1]. However, getting specific driving scenarios in particular adverse weather conditions can be challenging and time consuming. For example, collecting specific scenarios in heavy snowy conditions not only demands specific seasonal time, that can be rarely achieved across years, but it can also cause LiDAR sensor contamination from snow accumulation. Additionally, manually annotating ground truth can also be challenged by heavy occlusion of objects. For this reason, several datasets [2], [3] lack adverse weather conditions scenarios. On the other hand, previous research tried to work on the other way around and denoising adverse weather scenarios, as in the case of snowfall in [4]. While this work successfully removes snow clutter noise, it still suffers from heavy occluded objects. Compared to methods based on denoising, adverse weather data augmentation methods demonstrate superior effectiveness and accuracy in terms of downstream perception performance [5], [6]. In our work, we focus on the generation of heavy snowy conditions augmentation data. We work with the Boreas dataset [7], as it contains a repeated route in both sunny and snowy conditions. However, we do not explicitly leverage the

availability of close matching sunny and snowy scenes during the training, but rather for the evaluation of our method. Our method can work with diverse sunny and snowy scenes and it allows generalization capabilities of the adverse weather conditions augmentation. Our method comprises a latent diffusion process, including novel autoencoder and latent diffusion models (LDMs), aiming to recover the structure and add the adverse weather conditions to clear weather scenarios. A postprocessing step is further derived in order to recover fine-grained details of the generated adverse weather scenes, leveraging the corresponding clear weather input scenes. Because of the complex details of heavy snowy conditions, we (plan to) quantitatively prove the effectiveness of our augmentation method with a 3D object detection model, CenterPoint [8]. We separately train the model with sunny scenes augmented with our generated snow and with only sunny scenes, and validate both the models on real snowy scenarios. The repeated route among both the weather conditions scenes allows to disentangle the generalization capabilities of the trained model across different scenarios, to the capacity of the model to learn the generated snow distribution patterns. This permits to directly correlate improvements of the model, trained on the augmented data, to the capability of our method to generate snow that resembles the real one.

In summary, our key contributions are:

- We propose a novel procedure to augment clear scenes with adverse weather conditions.
- We introduce a novel autoencoder and conditioned latent diffusion model to learn distributions of adverse weather conditions.
- We introduce a novel postprocessing method to leverage the input clear weather scenes and improve the generated adverse weather scenes with fine-grained details.
- We (plan to) validate our components with distance-based and statistical metrics and we (plan to) validate our augmentation with 3D object detection.

II. RELATED WORK

A. Adverse Weather Conditions

The problem of generating adverse weather conditions for LiDAR scenes is still under explored. Previous works [5], [9]

tried to generate snowy conditions with methods based on CycleGAN [10]. However, diffusion models [11] demonstrate better generation results than generative adversarial networks (GANs) in image synthesis [12].

III. OUR METHOD

Our method takes as input a clear weather range image of the 3D point cloud) and generates adverse weather through a latent diffusion process. Our autoencoder generates discrete latent space with a latent quantization (LQ) layer. Moreover, the latent space is diffused and denoised for t steps by our latent diffusion models. The denoising process is guided by adverse conditioning, which is handled by feature-wise linear modulation ($FiLM$) layers. These layers process the adverse conditioning to guide the generation of a latent space representing adverse weather while recovering the underlying structure of the clear weather scene. Finally, the adverse weather latent space is reconstructed with the autoencoder. The resulting adverse weather scene is refined with a post-processing step, leveraging the input clear weather scene (see Fig. 1).

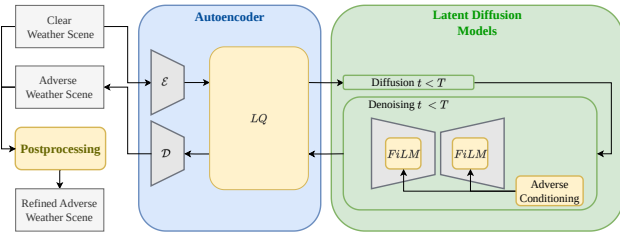


Fig. 1: Our method, constituted by autoencoder, latent diffusion models and postprocessing. We highlight in yellow our main contributions.

A. Data Representation

In order to efficiently learn latent spaces via autoencoder and use diffusion models, we project point clouds in 2D depth range images $x \in \mathbb{R}^{H \times W}$. The Boreas dataset [7] contains scenes recorded with a 128-channel Velodyne Alpha Prime LiDAR. Differently from LiDAR sensors used in KITTI [2] and nuScenes [3], the beams of this sensor are not equally partitioned along the elevation ϕ . For this reason, we partition the elevation, along the image height H , based on the point-wise beam id $\in [0, 127]$ instead of uniformly partitioning the elevation in equal $\Delta\phi$. The azimuth θ is instead uniformly partitioned in equal $\Delta\theta$, along the image width W . The final projection is a one channel 128×1024 range image and each pixel corresponds to the normalized point depth $d \in [-1, 1]$ (see Fig. 2).

B. Autoencoder

Inspired by the autoencoder proposed in [13], we introduce an autoencoder that is trained on data from both clear and adverse weather conditions. A fundamental component of [13] is the vector quantization (VQ) derived from [14], [15].

This component, interlayed between the encoder \mathcal{E} and the decoder \mathcal{D} , allows to map encoded vectors of the continuous latent space (pre-quantized latent space) to a discrete space of learnable vectors in the form of a discrete spatial codebook. The mapping is achieved though a vector-wise $\arg \min$ and generates a quantized latent space. Formally, given a range image $x \in \mathbb{R}^{H \times W}$, the encoder \mathcal{E} performs a mapping $z = \mathcal{E}(x) \in \mathbb{R}^{h \times w \times n_z}$, where $h = H/f_h$, $w = W/f_w$, with f_h, f_w scaling factors, and n_z is the dimensionality of each spatial code $z_{ij} \in \mathbb{R}^{n_z}$. Given a learnable discrete codebook $Z = \{z_k\}_{k=1}^K \subset \mathbb{R}^{n_z}$, VQ performs a vector-wise mapping of each z_{ij} :

$$z_q^{VQ} = VQ(z) := \left(\arg \min_{z_k \in Z} \|z_{ij} - z_k\| \right) \in \mathbb{R}^{h \times w \times n_z}. \quad (1)$$

This discrete space helps to prevent overfitting and, compared to the continuous pre-quantized latent space, provides a simpler distribution for downstream latent diffusion models to learn from [14], [16]. However, when trained on clear and adverse weather conditions, this discrete latent space does not guarantee that two similar static scenes, differing only for weather conditions, are also close in the quantized latent space. To achieve this similarity, we need to enforce a disentanglement of the codebook, in order to force the latent space to encode the adverse weather as a disentangled feature of the vectorized latent space. Following the research of [17], we use a disentangled quantization called latent quantization (LQ). Thus, instead of learning a vector-wise codebook, we learn component-wise scalar codebooks. Each component of spatial codes z_{ij} is mapped through a component-wise $\arg \min$ over the corresponding component-wise codebook. Formally, we define each scalar codebook as a set $C_n = \{c_r \in \mathbb{R} | r = 1, \dots, r_c\}$ of r_c learnable real numbers. A spatial code vector $z_{ij} \in \mathbb{R}^{n_z}$ can be represented as the cartesian product of n_z distinct scalar codebooks $z_{ij} = \prod_{n=1}^{n_z} C_n := C_1 \times \dots \times C_{n_z}$. Given n_z learnable scalar codebooks, LQ performs a component-wise mapping of each z_{ij} :

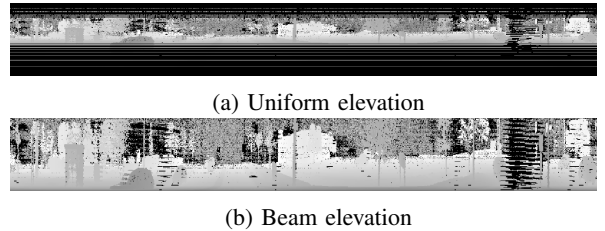


Fig. 2: Adverse weather depth range image. (a) with uniform elevation partition, (b) with beam id partition (ours).

$$z_l = \left(\prod_{n=1}^{n_z} \arg \min_{c_r \in C_n} \|z_{ij_n} - c_r\| \right) \in \mathbb{R}^{h \times w \times n_z},$$

$$z_q^{LQ} = LQ(z) := z + \text{StopGradient}(z_l - z) \in \mathbb{R}^{h \times w \times n_z}. \quad (2)$$

LQ provides greater expressiveness by allowing combinatorial selection of the components in its codebooks. By limiting the total number of learnable scalar values in each codebook, we can enforce the autoencoder to disentangle the latent space and to assign similar components to inputs sharing corresponding similar scene features. In this way, similar scenes that differ only in weather conditions exhibit the same behavior in the quantized latent space. Forcing adverse weather into a specific vector component enables the encoding of unique features of different weather conditions and prevents the loss of high-frequency details. Moreover, forcing the latent space to map input scene features to specific vector components allows the decoder to focus independently on different scenes features [17]. Finally, disentangled adverse weather conditions allows conditioned diffusion models to associate particular distributions of the latent space to corresponding adverse weather conditions. To learn meaningful latent spaces, the autoencoder is trained on a reconstruction loss \mathcal{L}_{rec} between the input $x \in \mathbb{R}^{H \times W}$ and the reconstruction \hat{x} :

$$\hat{x} = \mathcal{D}(z_q^{LQ}) = \mathcal{D}(LQ(\mathcal{E}(x))) \in \mathbb{R}^{H \times W}. \quad (3)$$

We use only \mathcal{L}_I loss as reconstruction:

$$\mathcal{L}_{rec}(x) = \mathbb{E}_x \|x - \hat{x}\|. \quad (4)$$

This allows to prevent overfitting, especially with adverse weather conditions reconstruction. On the other hand, relying only on \mathcal{L}_I loss limits the reconstructions of high-frequency details, since this loss focuses on low-frequency details by operating in pixel-wise distances. However, the autoencoder is trained in order to recover the structure and adverse weather conditions, while the postprocessing can restore fine-grained details. In order to learn disentangled codebooks, the autoencoder is also trained with $\mathcal{L}_{quantize}$ and \mathcal{L}_{commit} [14], [15], [17]:

$$\mathcal{L}_{quantize} = \left\| \text{StopGradient}(z) - z_q^{LQ} \right\|_2^2, \quad (5)$$

$$\mathcal{L}_{commit} = \left\| z - \text{StopGradient}(z_q^{LQ}) \right\|_2^2. \quad (6)$$

$\mathcal{L}_{quantize}$ moves the quantized vectors z_q^{LQ} towards the encoder outputs z and \mathcal{L}_{commit} makes sure the encoder commits to a latent space [14]. The total loss \mathcal{L} of the autoencoder is:

$$\mathcal{L} = \mathcal{L}_{rec} + \mathcal{L}_{quantize} + \mathcal{L}_{commit}. \quad (7)$$

C. Latent Diffusion Models

Latent diffusion models [11] and more recent stable diffusion [18] learn distribution of the discrete quantized latent space in order to generate latent vectors to be decoded by the pre-trained autoencoder. The generation of latent vectors can be guided towards specific conditions [19]. Stable diffusion

[18] conditions the diffusion model through cross-attention layers [20] along a temporal embedding of the denoising step, combined with a conditioning embedding. The use of cross-attention allows to learn strong relations between specific distributions of the latent space and the specific conditioning. In particular, the attention mechanism enables the learning of local and fine-grained dependency features. This requires a large amount of data. In adverse weather conditions, the scarcity of data, combined with the assumption that adverse weather acts as a global feature along the range image, leads us to simplify the handling of the conditioning. Starting from the architecture of stable diffusion, we replace cross-attention modules with feature-wise linear modulation ($FiLM$) layers [21]. These layers are applied as intermediate modules along the U-net architecture of the diffusion model. Taking as input the time embedding e_t concatenated with an adverse conditioning in the form of a binary label b (0 for clear and 1 for adverse), this layer learns a time-dependent conditioned linear modulation of the intermediate activations. This is achieved by learning functions f_i and h_i which output $\gamma_i, \beta_i \in \mathbb{R}^{n_i}$, that are globally applied along the intermediate activations $a_i \in \mathbb{R}^{h_i \times w_i \times n_i}$:

$$\gamma_i = f_i(e_t \oplus b) \quad \beta_i = h_i(e_t \oplus b), \quad (8)$$

$$FiLM(a_i | e_t \oplus b) = \gamma_i a_i + \beta_i.$$

$FiLM$ allows to learn global features of adverse weather conditions, and the linearity of the layer does not require huge amount of adverse weather inputs to learn distinctive features between clear and adverse weather conditions. We train the diffusion model on both clear and adverse weather conditions scenes for a number of steps T with classifier-free guidance [22]. The generation of latent space, derived from an iterative denoising process, is usually initialized from gaussian noise. In our augmentation method, we want to add adverse weather condition features without losing the specific scene environment. By diffusing clear weather latent spaces for a number of steps $t < T$ we can preserve feature details of the original scene and by denoising the noisy latent space for t steps through the diffusion model, conditioned on snow ($b = 1$), we can recover the input scene structure and add the adverse weather condition features.

D. Postprocessing

Latent spaces inherently discard high-frequency details because of their lower dimensionality space [18], compared to the original scene $x \in \mathbb{R}^{H \times W}$. During the latent diffusion process, the t steps of diffusion and denoising of input latent space further degrades high-frequency details and the corresponding decoded adverse weather scene $y \in \mathbb{R}^{H \times W}$ intrinsically lacks fine-grained details. Our postprocessing step leverages input clear scenes, and by distinguishing adverse features from static environment, recovers fine-grained details of the scenes while preserving the generated adverse weather conditions. Scenes generated from the latent diffusion process recover the static environment of corresponding clear scenes with the addition of adverse weather features. In the range

image domain, pixels of the generated adverse weather scene representing recovered static environment are more similar to corresponding input clear scene pixels, compared to pixels representing adverse weather features. Additionally, adverse weather features decreases for the increasing sparsity of point clouds in higher depth. By deriving a depth-dependent threshold $d_t \in \mathbb{R}^{H \times W}$, we can distinguish adverse weather features from the static environment at the pixel level. In particular, this threshold increases for higher depth as adverse weather features decrement, combined with the decremental precision of the latent diffusion process in recovering the structure for higher depth. By matching depths of the input clear weather scene $d_x \in \mathbb{R}^{H \times W}$ and the corresponding augmented adverse weather scene $d_y \in \mathbb{R}^{H \times W}$, we can take pixels representing static environment from the input clear weather scene x and pixels representing occluding adverse weather features from the augmented adverse weather scene y . The postprocessing method is given in Algo. 1. In lines 1-2, we define d_x and d_y as the unnormalized absolute pixel-wise depths of respectively x and y . Moreover, in line 3 we define d_t as a pixel-wise parametrized exponential function, increasing with the depth d_y . A parametrized exponential function ensures low threshold values for shallow depths and a progressive increase for greater depths. In this manner, snow features are preserved at lower depths, while fine-grained details are recovered at greater depths. Finally, in line 9, $minDepth$ selects the adverse pixel $y[i]$ only if it constitutes occlusion (lower depth than $x[i]$).

Algorithm 1: Postprocessing

Data:

$x \leftarrow$ input clear weather scene
 $y \leftarrow$ augmented adverse weather scene
 $\lambda, \nu \leftarrow$ depth threshold parameters

Input: x, y

Output: Refined augmented adverse weather scene y'

```

1  $d_x \leftarrow Depth(x)$ 
2  $d_y \leftarrow Depth(y)$ 
3  $d_t \leftarrow exp(d_y, \nu) \cdot \lambda$ 
4  $\delta = abs(d_x - d_y)$ 
5 for  $i \in shape(\delta)$  do
6   if  $\delta[i] < d_t[i]$  then
7      $y'[i] \leftarrow x[i]$ 
8   else
9      $y'[i] \leftarrow minDepth(x[i], y[i])$ 
10 return  $y'$ 

```

IV. EXPERIMENTS

A. Evaluation Metrics

The Chamfer distance (CD) and the Jensen-Shannon divergence (JSD) are two common metrics to evaluate reconstruction fidelity of 3D point clouds [13], [23]. The CD evaluates the completion at point level, measuring the level of detail of the reconstructed scene by calculating how far are its points

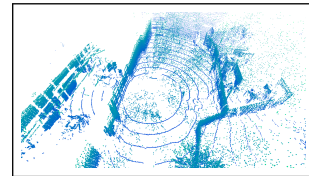
from the ground truth scene. The JSD is a statistical metric that compares the points distribution between the reconstruction and the ground truth scene. Differently from previous work, we applied the JSD on the 3D voxelized scenes without projecting to a birds-eye view (BEV). Additionally, we set a grid resolution of 0.15m. This because we want to assess the 3D adverse weather reconstruction quality.

B. Autoencoder

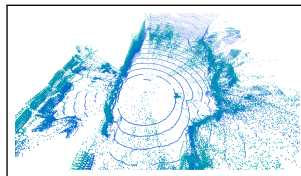
We trained autoencoders with both VQ and LQ quantizations. We set the scaling factors $f_h = 4, f_w = 8$, and the dimensionality of each spatial code $n_z = 16$ such that $z_q^{VQ}, z_q^{LQ} \in \mathbb{R}^{32 \times 128 \times 16}$. For VQ , the total number of learnable vectors in the learnable discrete codebook is $|Z| = 16384$ and the total number of learnable values is therefore $|Z| \cdot n_z = 262,144$. For LQ , each of the n_z learnable scalar codebooks learns $|C_n| = 256$ scalar values and the total number of learnable values is therefore $|C_n| \cdot n_z = 4096$. We evaluate both autoencoders in sunny and snowy scene reconstructions. As shown in Table I, LQ outperforms VQ in the reconstruction of both sunny and snowy scenes. In both autoencoders, the reconstruction of snowy scenes is more challenging than sunny scenes. From Fig. 3, LQ demonstrates higher quality of snow reconstruction. In both reconstructions, the scene structure degrades with increasing depth but the overall structure is recovered.

TABLE I: Performance of autoencoders VQ (baseline) and LQ (ours) in sunny and snowy reconstructions.

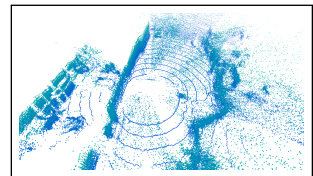
Method	sun		snow	
	CD↓	JSD↓	CD↓	JSD↓
VQ (baseline)	0.276	0.691	0.281	0.692
LQ (ours)	0.181	0.647	0.194	0.659



(a) Original scene



(b) VQ (baseline)



(c) LQ (ours)

Fig. 3: Snowy weather scene (a) and reconstructions (b), (c).

REFERENCES

[1] Mariella Dreissig, Dominik Scheuble, Florian Piewak, and Joschka Boedecker. Survey on lidar perception in adverse weather conditions. In *2023 IEEE Intelligent Vehicles Symposium (IV)*, pages 1–8. IEEE, 2023.

- [2] Andreas Geiger, Philip Lenz, and Raquel Urtasun. Are we ready for autonomous driving? the kitti vision benchmark suite. In *2012 IEEE conference on computer vision and pattern recognition*, pages 3354–3361. IEEE, 2012.
- [3] Holger Caesar, Varun Bankiti, Alex H Lang, Sourabh Vora, Venice Erin Liong, Qiang Xu, Anush Krishnan, Yu Pan, Giancarlo Baldan, and Oscar Beijbom. nuscenes: A multimodal dataset for autonomous driving. In *Proceedings of the IEEE/CVF conference on computer vision and pattern recognition*, pages 11621–11631, 2020.
- [4] Nicholas Charron, Stephen Phillips, and Steven L Waslander. De-noising of lidar point clouds corrupted by snowfall. In *2018 15th Conference on Computer and Robot Vision (CRV)*, pages 254–261. IEEE, 2018.
- [5] Yuxiao Zhang, Ming Ding, Hanting Yang, Yingjie Niu, Maoning Ge, Kento Ohtani, Chi Zhang, and Kazuya Takeda. Lidar point cloud augmentation for adverse conditions using conditional generative model. *Remote Sensing*, 16(12):2247, 2024.
- [6] Martin Hahner, Christos Sakaridis, Mario Bijelic, Felix Heide, Fisher Yu, Dengxin Dai, and Luc Van Gool. Lidar snowfall simulation for robust 3d object detection. In *Proceedings of the IEEE/CVF conference on computer vision and pattern recognition*, pages 16364–16374, 2022.
- [7] Keenan Burnett, David J Yoon, Yuchen Wu, Andrew Z Li, Haowei Zhang, Shichen Lu, Jingxing Qian, Wei-Kang Tseng, Andrew Lambert, Keith YK Leung, et al. Boreas: A multi-season autonomous driving dataset. *The International Journal of Robotics Research*, 42(1-2):33–42, 2023.
- [8] Tianwei Yin, Xingyi Zhou, and Philipp Krähenbühl. Center-based 3d object detection and tracking. *CVPR*, 2021.
- [9] Yuxiao Zhang, Ming Ding, Hanting Yang, Yingjie Niu, Yan Feng, Kento Ohtani, and Kazuya Takeda. L-dig: A gan-based method for lidar point cloud processing under snow driving conditions. *Sensors*, 23(21):8660, 2023.
- [10] Jun-Yan Zhu, Taesung Park, Phillip Isola, and Alexei A Efros. Unpaired image-to-image translation using cycle-consistent adversarial networks. In *Proceedings of the IEEE international conference on computer vision*, pages 2223–2232, 2017.
- [11] Jonathan Ho, Ajay Jain, and Pieter Abbeel. Denoising diffusion probabilistic models. *Advances in neural information processing systems*, 33:6840–6851, 2020.
- [12] Prafulla Dhariwal and Alexander Nichol. Diffusion models beat gans on image synthesis. *Advances in neural information processing systems*, 34:8780–8794, 2021.
- [13] Haoxi Ran, Vitor Guizilini, and Yue Wang. Towards realistic scene generation with lidar diffusion models. In *Proceedings of the IEEE/CVF Conference on Computer Vision and Pattern Recognition*, pages 14738–14748, 2024.
- [14] Aaron Van Den Oord, Oriol Vinyals, et al. Neural discrete representation learning. *Advances in neural information processing systems*, 30, 2017.
- [15] Patrick Esser, Robin Rombach, and Bjorn Ommer. Taming transformers for high-resolution image synthesis. In *Proceedings of the IEEE/CVF conference on computer vision and pattern recognition*, pages 12873–12883, 2021.
- [16] Ze Wang, Jiang Wang, Zicheng Liu, and Qiang Qiu. Binary latent diffusion. In *Proceedings of the IEEE/CVF conference on computer vision and pattern recognition*, pages 22576–22585, 2023.
- [17] Kyle Hsu, William Dorrell, James Whittington, Jiajun Wu, and Chelsea Finn. Disentanglement via latent quantization. *Advances in Neural Information Processing Systems*, 36, 2024.
- [18] Robin Rombach, Andreas Blattmann, Dominik Lorenz, Patrick Esser, and Björn Ommer. High-resolution image synthesis with latent diffusion models. In *Proceedings of the IEEE/CVF conference on computer vision and pattern recognition*, pages 10684–10695, 2022.
- [19] Lvmin Zhang, Anyi Rao, and Maneesh Agrawala. Adding conditional control to text-to-image diffusion models. In *Proceedings of the IEEE/CVF International Conference on Computer Vision*, pages 3836–3847, 2023.
- [20] A Vaswani. Attention is all you need. *Advances in Neural Information Processing Systems*, 2017.
- [21] Ethan Perez, Florian Strub, Harm De Vries, Vincent Dumoulin, and Aaron Courville. Film: Visual reasoning with a general conditioning layer. In *Proceedings of the AAAI conference on artificial intelligence*, volume 32, 2018.
- [22] Jonathan Ho and Tim Salimans. Classifier-free diffusion guidance. *arXiv preprint arXiv:2207.12598*, 2022.
- [23] Lucas Nunes, Rodrigo Marcuzzi, Benedikt Mersch, Jens Behley, and Cyrill Stachniss. Scaling diffusion models to real-world 3d lidar scene completion. In *Proceedings of the IEEE/CVF Conference on Computer Vision and Pattern Recognition*, pages 14770–14780, 2024.